

Flat Lenses

Tracing the Evolution from Smooth Surfaces to Fresnel,
Diffractive, and Metalenses

Frank Wyrowski

January 2025

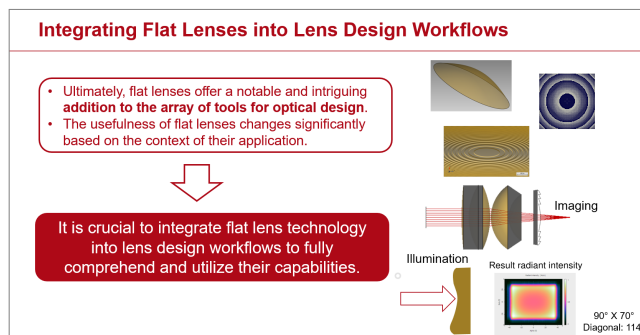
Abstract

Smooth interfaces between two media are typically used to shape wavefronts in optical design. Spherical and aspherical interfaces are utilized in the creation of lenses and mirrors in imaging systems. In nonimaging optics, free-form surfaces are employed to deliberately introduce particular aberrations to shape the energy distribution of light. In every scenario, the surface performs a transformation of the incoming wavefront's phase into a specific output phase that aligns with the design criteria.

Flat surfaces can be utilized to achieve the same phase transformations that are typically conducted with smooth surfaces. This paper explores the fundamental principles involved in designing flat lenses, including Fresnel lenses, diffractive lenses, and metalenses.

All illustrative instances are performed using VirtualLab Fusion (VLF) software. The newly introduced techniques and features are planned for release to VLF in 2025. Reach out to support@lighttrans.com for additional release details and any inquiries you may have concerning metalens design and modeling.

This paper derives from the transcript and slides of the webinar "Flat Lenses: Tracing the Evolution from Smooth Surfaces to Fresnel, Diffractive, and Metalenses," presented by Frank Wyrowski at the Photonics Media webinar on May 22, 2024. Consult the slides.pdf file to view all slide images.



1 Potential and Limitations of Flat Lenses

Slides #2–5

At the beginning of this paper, I intend to tackle the question: What results can be expected from integrating flat lenses into optical design? To address this question, it is helpful to introduce some basic principles of lens design relevant to the discussion on flat lenses. Every lens is designed to transform one or more incoming wavefronts. In imaging, it is common to transform spherical and planar wavefronts. The function of a lens is defined by the transformations it is intended to execute. This information is preserved and accessible for modeling and design through what is known as a functional lens. A functional lens provides details on all transformations through a collection of input phases and their corresponding outputs, also known as signal phases. A transformation that involves just one pair of wavefront phases is termed a single-field transformation. On the other hand, when multiple pairs of wavefront phases are involved, the process is referred to as a multifield transformation.

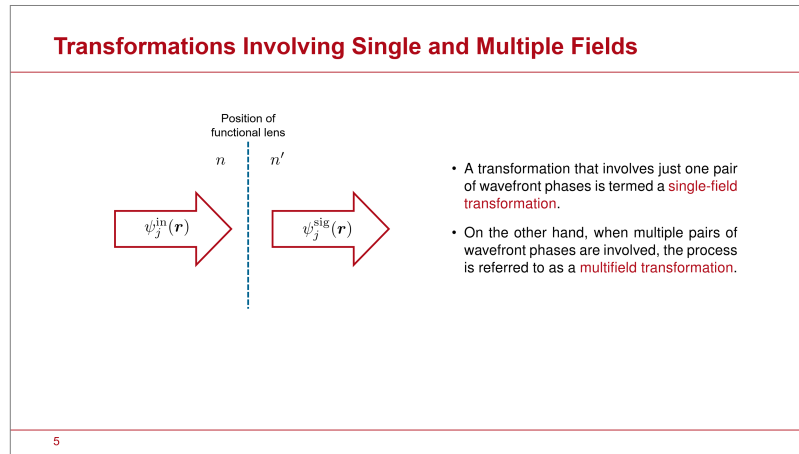


Figure 1: Slide #5

Slides #6–7

In a basic imaging scenario, the functional lens specifies the transformation of divergent spherical input wavefront phases into convergent spherical output wavefront phases. This paper will concentrate on transformations associated with monochromatic light. I recommend referring to a work by Kleemann et al., which provides insights into designing flat optics for polychromatic light, based on techniques applied to monochromatic light [2].

Beginning with the specifications of the functional lens, the goal in designing the lens surface is to substitute a functional lens with a physical lens that achieves the designated single- or multi-field transformation. Within the paraxial approximation, the design of the surface is resolved by a single spherical surface.

Slides #8–13

Let us examine in detail the design of a single lens surface that achieves a single-field

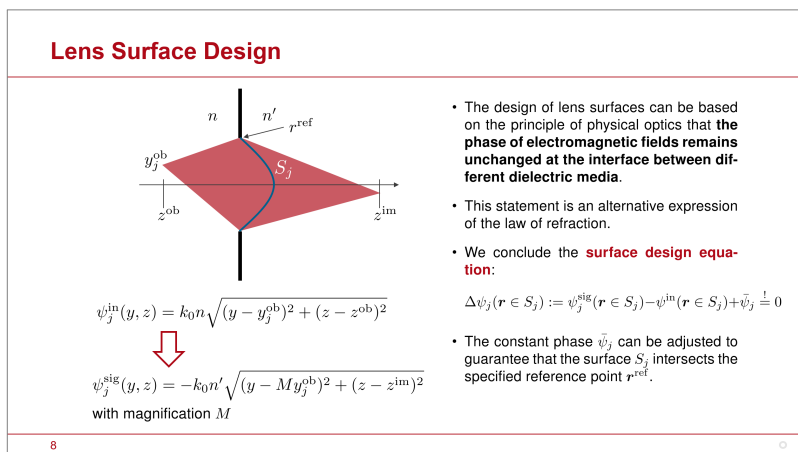


Figure 2: Slide #8

transformation. The design of lens surfaces can be based on the principle of physical optics that the phase of electromagnetic fields remains unchanged at the interface between different dielectric media. This statement is an alternative expression of the law of refraction. We conclude the surface design equation:

$$\Delta\psi_j(\mathbf{r} \in S_j) := \psi_j^{\text{sig}}(\mathbf{r} \in S_j) - \psi_j^{\text{in}}(\mathbf{r} \in S_j) + \bar{\psi}_j \stackrel{!}{=} 0 \quad (1)$$

The constant phase $\bar{\psi}_j$ can be adjusted to guarantee that the surface S_j intersects the specified reference point \mathbf{r}^{ref} .

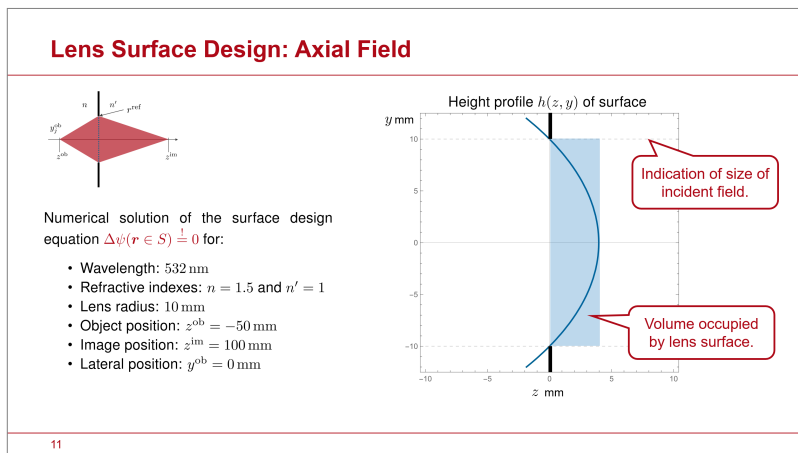


Figure 3: Slide #11

We start with the example specified in Fig. 3. Solving the design equation numerically results in the surface S , which achieves the desired transformation. The dashed line indicates the size of the incoming field, and from this we determine the surface thickness as depicted in the blue region. It is important to note that flattening the

lens surface does not affect the distances to the object and image planes, and thus, the system's length remains unchanged.

Slides #14–16

Next, let's examine an off-axis field and proceed with the surface design using two different reference points. The surfaces obtained are illustrated in Fig. 4. As anticipated, the surfaces generated by various object points are somewhat distinct. Thus, a single surface fails to address multifield transformations and generates aberrations for any input wavefront other than the one it was designed for. Hence, it is essential to include extra surfaces to balance aberrations and achieve the required multi-field transformation with adequate precision. There is no evidence to suggest that flat lenses eliminate this requirement.

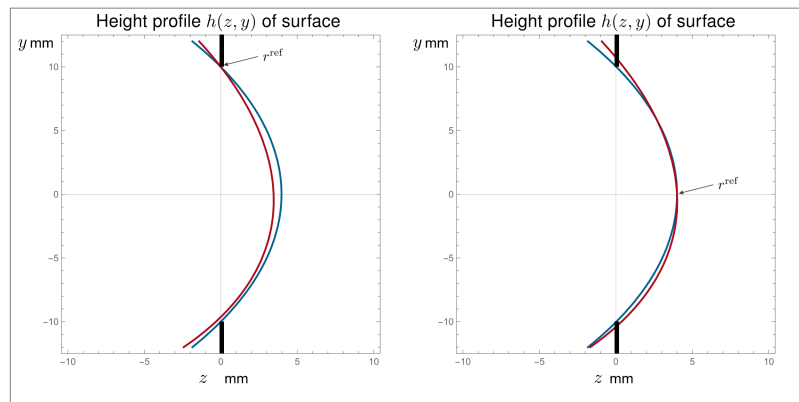


Figure 4: Surface designs for on-axis (blue) and off-axis (red) object points for two different reference points.

Imaging Example: Telecentric Image Side

- It should be noted that there are mentions of configurations in which fields overlap yet occupy separate regions as a method to correct aberrations of flat lenses.
- Certainly, designing lens surfaces for aberration control near image planes offers benefits over lenses positioned near the stop and pupils. However, this applies equally to both flat and "thick" lens surfaces.

Example of cell phone lens system

17

Figure 5: Slide #17

Slides #17–18

It should be noted that in literature are mentions of configurations in which fields overlap yet occupy separate regions as a method to correct aberrations of flat lenses. Certainly, designing lens surfaces for aberration control near image planes offers benefits over lenses positioned near the stop and pupils. However, this applies equally to both flat and "thick" lens surfaces. This becomes clearly evident with the example of the cell phone camera lens system in Fig. 5.

To gain further insight, let's consider the design of a beam expander. In this case, an initial lens is necessary to transform the incoming planar phase into either a converging or diverging spherical phase. The divergent case is demonstrated. A second lens is utilized to collimate the incoming light, thereby transforming the spherical phase back into a planar phase. Thus, the use of two lenses is necessary. The degree of beam expansion is governed by the distance d between the lenses and their numerical apertures. Flattening the lenses does not change that outcome.

Slides #19–29

These observations lead to the following conclusions:

- Flat lenses reduce both the thickness and weight of the lenses.
- The slim profile of flat lenses might enable more options for decreasing the spacing between lens surfaces.
- The fabrication methods for flat lenses vary from those for traditional lenses, which may offer benefits in specific scenarios.
- Flat lenses could provide new opportunities for switchable lenses.
- Replacing thick lens surfaces with flat surfaces changes the aberration dynamics in the system, which may enhance aberration correction possibilities based on the particular scenario.
- Employing diffractive lenses, which exhibit strong and opposing chromatic aberrations, to counteract the chromatic aberrations of smooth lens surfaces serves as a well-documented instance of this potential.
- Some characteristics of flat lenses, such as its polarization-sensitive function, may be considered beneficial or detrimental depending on their use.
- There is no evidence to suggest that flat lenses, including metalenses, reduce the total length of the system or the number of lens surfaces in optical systems beyond what is possible with aspherical and freeform surfaces.¹

Slides #30–38

Ultimately, flat lenses offer a notable and intriguing addition to the array of tools for

¹In this context, we omit any possible minor decrease in the system's length caused by the second item in the list.

optical design. The usefulness of flat lenses changes significantly based on the context of their application. In conclusion, it is crucial to integrate flat lens technology into lens design workflows to fully comprehend and utilize their capabilities. It is time to practically evaluate the potential of flat lenses and move beyond mere theoretical debates. The following two workflows are of paramount importance: Workflow #1:

1. Carry out the structural design of a flat lens based on a specified functional lens.
2. Evaluate the performance of the flat lens.
3. Collect and export lens data for manufacturing needs.

Workflow #2:

1. Substitute a 'thick' lens surface with a flat lens.
2. Assess the functioning of the system that incorporates the flat lens.
3. Facilitate system optimization.

Incorporation of flat lenses into lens design workflows requires substantial advances in both theoretical underpinnings and the implementation of optics software. Introducing data interfaces across various software products does not offer the required solution.

Three essential objectives must be achieved in the advancement of optics software:

1. Develop efficient and user-friendly design algorithms for flat lenses.
2. Enable the simulation of lens systems that incorporate flat lenses with adequate accuracy and speed.
3. Facilitate the optimization of optical systems that incorporate flat lenses.

At LightTrans, we are committed to enhancing the flat-lens features of our software, VirtualLab Fusion, to meet these objectives by 2025. This article concentrates on the initial objective. For a comprehensive exploration of all objectives, please refer to our paper on metalenses [6].

2 Design of Flat Lens Height Profiles

Slides #39–46

Initially, we examine flat lenses that are constructed using height profiles. Our exploration of flat optics design begins by examining how a plane wave is transformed from an input direction vector $\hat{\mathbf{s}}^{\text{in}}$ to a signal direction vector $\hat{\mathbf{s}}^{\text{sig}}$. The appropriate surface design is determined using the surface design equation:

$$\Delta\psi(\mathbf{r} \in S) = \psi^{\text{sig}}(\mathbf{r} \in S) - \psi^{\text{in}}(\mathbf{r} \in S) + \bar{\psi} \stackrel{!}{=} 0 \quad (2)$$

Solving the design equation analytically results in a planar surface. This outcome is entirely expected. The dashed lines represent the incident beam, and the region where this beam intersects the planar interface is highlighted in blue. Reducing the width of this region clearly shows that the interface is available only in a minor portion of the required aperture. Hence, additional surfaces are required to achieve a flat solution. In addition to the solution we have, there exist alternative solutions that satisfy the design equation

$$\Delta\psi(\mathbf{r} \in S_j) \stackrel{!}{=} j\Delta m \cdot 2\pi, \quad (3)$$

because for phase values, $j\Delta m \cdot 2\pi$ is equivalent to 0 when $m = j\Delta m$ is an integer. The solutions shown in Fig 6 consist simply of parallel planes. The parameter Δm is used to control the spacing between these solutions, with a setting of $\Delta m = 1$ resulting in the smallest possible spacing. We now possess a sufficient number of solutions within the narrow blue region.

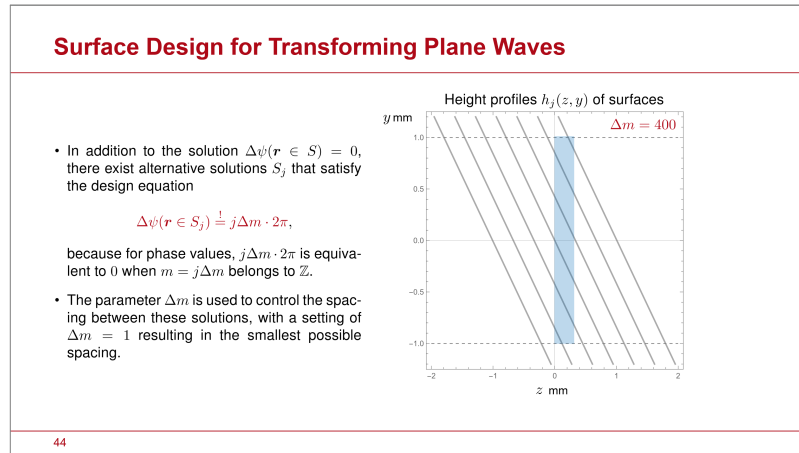


Figure 6: Slide #44

Slides #47–55

Based on the input direction vector, a triangle is formed using one plane, followed by successive constructions with additional planes in the blue area. This approach yields analytical formulas for the grating profile tailored to any given pair of input and output directions. The choice of Δm determines the height and period of the grating, with $\Delta m = 1$ achieving the minimum values for both. The method can be applied to both the transmission and reflection scenarios. This approach to grating design is scheduled for release in 2025 within VirtualLab Fusion.

Slides #56–59

We now proceed to discuss the broader scenario that involves transforming both planar and spherical phase profiles. Given that the transformation is specified by a functional lens, the shape of the lens surface is established through the numerical resolution of the surface design equation. The blue region indicates the depth of

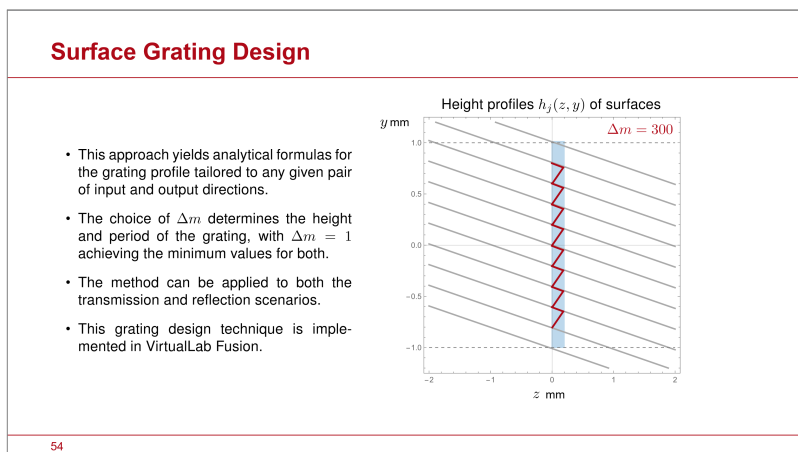


Figure 7: Slide #54

the lens surface. Reducing the thickness of this area evidently shows that in most of the thinner slab, there is no surface available to carry out the transformation. Additional surfaces S_j are required to achieve a flat lens and can be derived by numerical resolution of

$$\Delta\psi(\mathbf{r} \in S_j) \stackrel{!}{=} j\Delta m \cdot 2\pi, \quad (4)$$

where $m = j\Delta m$ is an integer (\mathbb{Z}). The parameter Δm is used to adjust the thickness of the flat lens, where setting $\Delta m = 1$ results in the thinnest possible configuration.

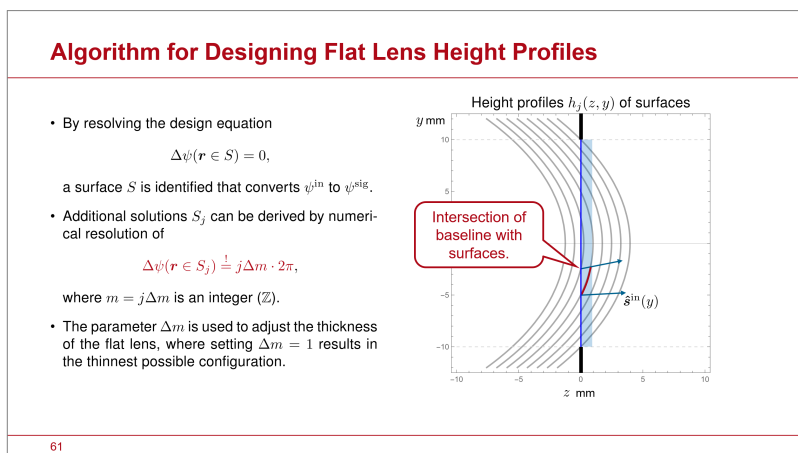


Figure 8: Slide #61

Slides #60–63

The flat lens design procedure starts by establishing a baseline and identifying the points where it intersects with the surfaces. At each intersection, a straight line is initiated following the local direction $\hat{\mathbf{s}}^{\text{in}} = \nabla\psi^{\text{in}}/(k_0 n)$ and the point where it intersects the subsequent surface is determined. By applying this method across the

entire lens aperture, the zones of the flat lens surface inside the thin slab are identified. This concept enables the creation of a quick and flexible algorithm for the design of flat lens surfaces. This method is applicable to scenarios involving both transmission and reflection and is effective regardless of whether rotational symmetry is assumed or not. The design algorithm is incorporated into our proprietary VirtualLab Fusion software and is scheduled to be released in an upcoming 2025 update.

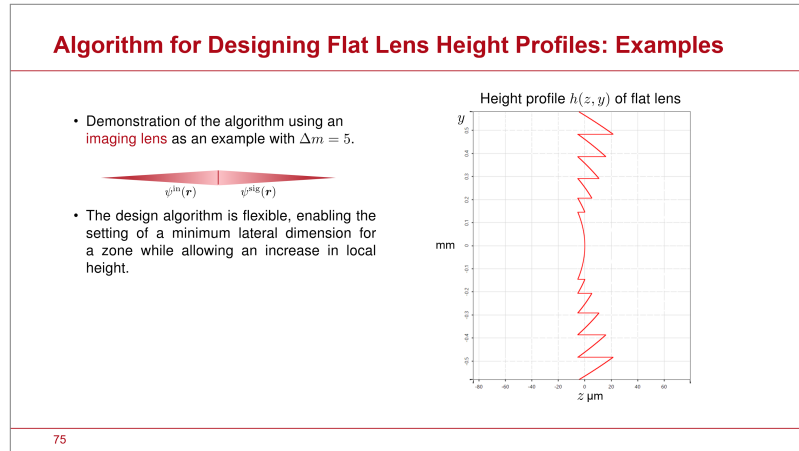


Figure 9: Slide #75

Slides #64–81

Let's now consider some sample applications of the design algorithm. Although the design method is highly applicable to practical scenarios, the examples provided are designed to demonstrate the functionality of the design algorithm for illustration purposes, rather than for direct real-world applications. First an example of a focusing lens with the baseline and the construction of the zones. In this case $\Delta m = 2$ leads to a lens thickness of about $2 \mu\text{m}$. In the following collimation scenario, choosing $\Delta m = 50$ achieves a lens thickness approximately $50 \mu\text{m}$. In this case the design leads to a noticeable tilt in the sidewalls. Next we consider an imaging example for the axial field. The design algorithm is flexible, enabling the setting of a minimum lateral dimension for a zone while allowing an increase in local height (see Fig: 9). This approach has been effectively implemented in the flat lenses used in Meta's Oculus VR glasses. The design algorithm allows for the distribution of lens power across both curved and flat lens surface profiles. To achieve this combination, we start with a curved baseline and follow the same procedure as that used for a straight baseline. Figure 10 shows an example.

Slides #82–84

The examples demonstrate that we developed a design algorithm tailored for flat lens height profiles. Flat lenses, which function according to their height profiles, are commonly known as:

- Fresnel lenses for large Δm

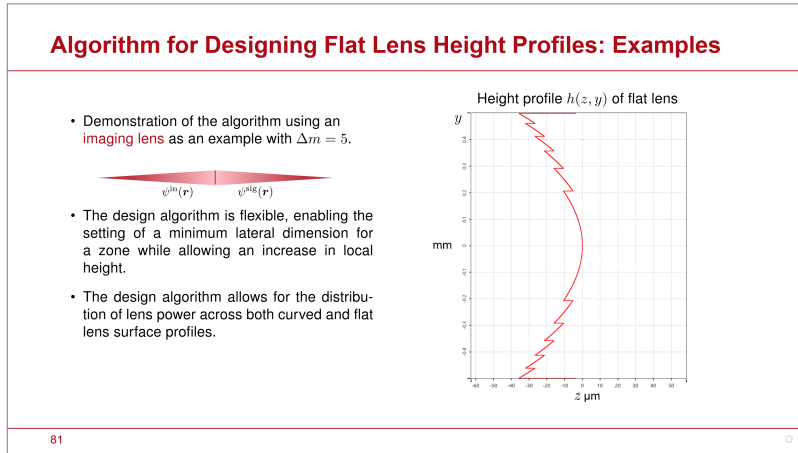


Figure 10: Slide #81

- diffractive lenses for $\Delta m = 1$
- superzone diffractive lens for small $\Delta m > 1$

For diffractive lenses, the height profile may be discretized to facilitate fabrication via binary lithography techniques. Next, we will discuss the design of flat lenses that utilize metasurfaces.

3 Design of Metalenses

Slides #85–88

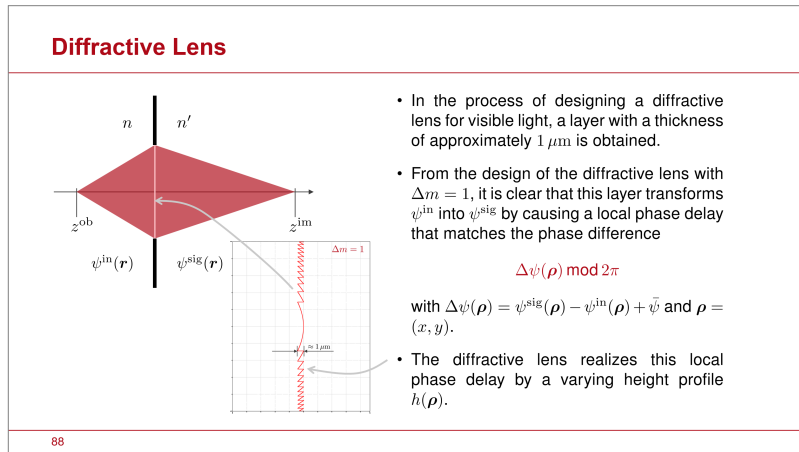


Figure 11: Slide #88

In the process of designing a diffractive lens for visible light, a layer with a thickness of approximately $1 \mu\text{m}$ is obtained. From the design of the diffractive

lens with $\Delta m = 1$, it is clear that this layer transforms ψ^{in} into ψ^{sig} by causing a local phase delay that matches the phase difference $\Delta\psi(\boldsymbol{\rho}) \bmod 2\pi$ with $\Delta\psi(\boldsymbol{\rho}) = \psi^{\text{sig}}(\boldsymbol{\rho}) - \psi^{\text{in}}(\boldsymbol{\rho}) + \bar{\psi}$ and $\boldsymbol{\rho} = (x, y)$. The diffractive lens realizes this local phase delay by a varying height profile $h(\boldsymbol{\rho})$ as illustrated in Fig. 11.

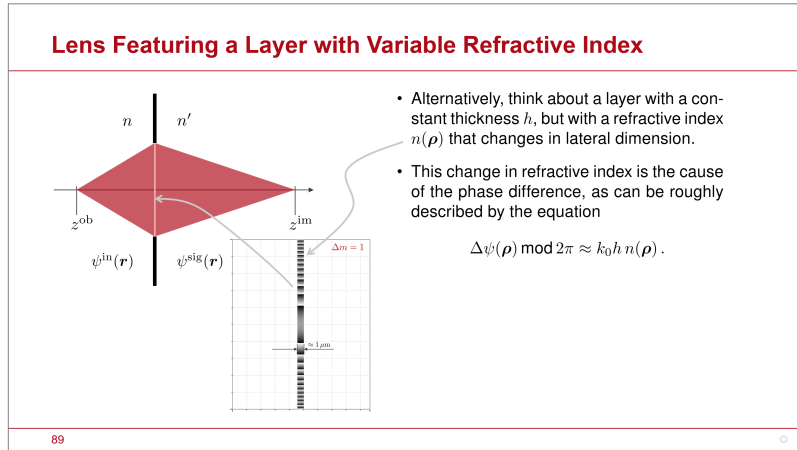


Figure 12: Slide #89

Slides #89–93

Alternatively, think about a layer with a constant thickness h , but with a refractive index $n(\boldsymbol{\rho})$ that changes in lateral dimension. Figure 12 demonstrates the scenario. The change in refractive index is the cause of the phase difference, as can be roughly described by the equation

$$\Delta\psi(\boldsymbol{\rho}) \bmod 2\pi \approx k_0 h n(\boldsymbol{\rho}). \quad (5)$$

To continue the discussion, we consider the index distribution in a two-dimensional space. Next, suppose that the lateral variation is implemented in a pixelated manner rather than continuously, leading to

$$\Delta\psi(\boldsymbol{\rho}_i) \bmod 2\pi \approx k_0 h n(\boldsymbol{\rho}_i), \quad (6)$$

with the positions $\boldsymbol{\rho}_i$ establishing an appropriate grid, such as a Cartesian grid. Metasurfaces utilize a high-refractive index nanostructure for each pixel placed on a substrate with a lower refractive index to achieve the local refractive index and associated phase shift. This concept requires that the distance between pixels, denoted as $\|\boldsymbol{\rho}_i - \boldsymbol{\rho}_{i+1}\|$, be less than the wavelength. The outcome yields a metasurface composed of appropriate nanostructures for each pixel.

Slides #94–100

This approach has been recognized for a while, but it has recently gained renewed interest [1, 3]. The process of generating phase delays is investigated through multiple theoretical approaches, differing in the type and form of the nanostructure used per pixel. For an initial insightful read, consider reading the review by Lalanne and

Chavel [4]. Additionally, the informative tutorial by Yang Fan et al. is recommended, which includes numerous additional references[5].

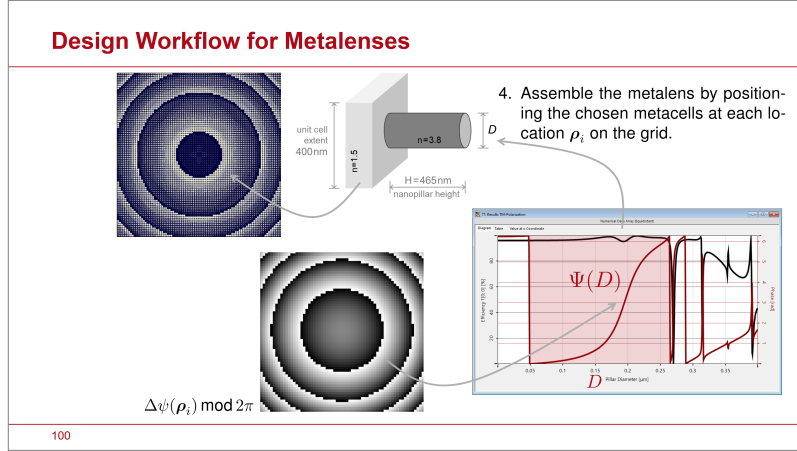


Figure 13: Slide #100

The fundamental steps involved in the design of metalenses include:

1. Choose a nanostructure, commonly known as a meta-atom or metacell, that aligns with the capabilities of your fabrication tools or collaborative partners.
2. Analyze the phase delay of the nanostructure dependent on the structure parameters $\mathbf{p} = (p_1, p_2, \dots)$, e.g. height, size, orientation, and obtain data on the phase delay $\Psi(\mathbf{p})$ of the metacell for the incident field $\mathbf{E}^{\text{in}} = \mathbf{U}^{\text{in}} \exp(i\psi^{\text{in}})$ in ρ_i .
3. Identify the parameters \mathbf{p} such that they satisfy the following condition for each pixel ρ_i :

$$\Psi(\mathbf{p}; \rho_i) = \Delta\psi(\rho_i) \bmod 2\pi \quad (7)$$
4. Assemble the metalens by positioning the chosen metacells at each location ρ_i on the grid.

Slides #101–102

The described design method for metasurfaces is available through VirtualLab Fusion software. The development is ongoing and new features are planned for future updates in 2025. Figure 14 illustrates an example that showcases the focusing ability of a metalens, constructed using the aforementioned algorithm.

Slides #103–117

Toward the conclusion of this discussion, we demonstrate an example in which we utilize the polarization sensitivity of a metalens made with rotated nanofins. For an in-depth analysis, please refer to our metalenses publication [6]. We position the metalens ahead of a thick lens and aim to investigate how the focus of the combined

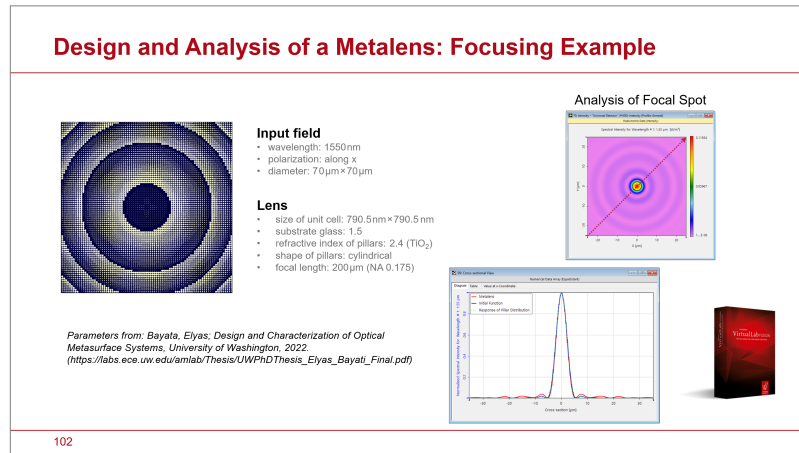


Figure 14: Slide #102

lenses varies based on the input polarization. The metalens is simulated through a quick and approximated model, demonstrating the polarization-sensitive focal length of the metalens while overlooking some effects of stray light. The modeling approach is compatible with the advanced fast lens system modeling technology used in VirtualLab Fusion. The selected **balance between modeling accuracy and speed** allows the simulation of the system in seconds. Initially, we present a simulation featuring a nanofin metalens followed by a functional focusing lens. The simulations provide both the ray paths and the irradiance distributions on the detection planes. To enhance the visibility of light on the second detector plane, we adjust the scale settings in that detector window. Changing the polarization to left circularly polarized light change the focus position. Switching to linearly polarized light results in the formation of two focal points. Next, we replace the functional focusing lens with a spherical one, using the lens maker equation. Significant spherical aberrations shift the focal points in this assembly, which includes a metalens and a spherical lens. To minimize aberrations, we substitute the spherical lens with an aspherical lens. We now obtain results that are nearly aligned with the functional lens. Refer to Fig. 15 for the outcomes obtained with linearly polarized incident light. The example serves as a demonstration of exploring the effectiveness of a metalens through a suitable selection of the balance between modeling accuracy and speed.

4 Conclusion

Slides #118

Flat lenses represent a significant and fascinating enhancement to the toolkit available for optical design, particularly in the fields of imaging and illumination. The effectiveness and utility of flat lenses are highly dependent upon the context in which they are applied. Ultimately, it is essential to incorporate flat lens technology into lens design workflows to fully grasp and take advantage of their potential. At LightTrans,

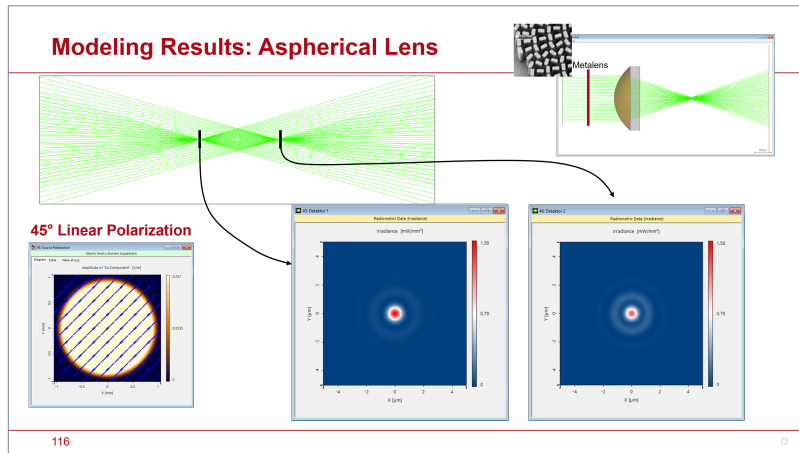


Figure 15: Slide #116

we are committed to significant advancements in achieving this important objective through our software VirtualLab Fusion in 2025. Stay tuned for more updates!

References

- [1] P. Lalanne et al. “Design and fabrication of blazed binary diffractive elements with sampling periods smaller than the structural cutoff”. In: *J. Opt. Soc. Am. A* 16.5 (1999), pp. 1143–1156.
- [2] Bernd H. Kleemann, Markus Seesselberg, and Johannes Ruoff. “Design concepts for broadband high-efficiency DOEs”. In: *Journal of the European Optical Society: Rapid Publications* 3 (2008), p. 08015. URL: <https://api.semanticscholar.org/CorpusID:55641984>.
- [3] Mohammadreza Khorasaninejad et al. “Metalenses at visible wavelengths: Diffraction-limited focusing and subwavelength resolution imaging”. In: *Science* 352.6290 (June 3, 2016), pp. 1190–1194. ISSN: 0036-8075, 1095-9203. DOI: [10.1126/science.aaf6644](https://doi.org/10.1126/science.aaf6644). URL: <https://www.science.org/doi/10.1126/science.aaf6644>.
- [4] Philippe Lalanne and Pierre Chavel. “Metalenses at visible wavelengths: past, present, perspectives”. In: *Laser & Photonics Reviews* 11.3 (May 2017), p. 1600295. ISSN: 1863-8880, 1863-8899. DOI: [10.1002/lpor.201600295](https://doi.org/10.1002/lpor.201600295). URL: <https://onlinelibrary.wiley.com/doi/10.1002/lpor.201600295>.
- [5] Fan Yang et al. “Wide field-of-view metalens: a tutorial”. In: *Advanced Photonics* 5 (May 1, 2023). ADS Bibcode: 2023AdPho...5c3001Y, p. 033001. DOI: [10.1117/1.AP.5.3.033001](https://doi.org/10.1117/1.AP.5.3.033001). URL: <https://ui.adsabs.harvard.edu/abs/2023AdPho...5c3001Y>.
- [6] Frank Wyrowski. *Integrating Metalens Modeling into Multiscale System Simulations*. 2025. URL: https://www.lighttrans.com/fileadmin/shared/VLF%20Technology/Technical_Insight_Integrating%20Metalens%20Modeling%20into%20Multiscale%20System%20Simulations_Article.pdf.